# Modelling and Simulation of Solar Plant and Storage System: A Step to Microgrid Technology

Jakir Hossain*, Nazmus Sakib**, Eklas Hossain***‡, Ramazan Bayindir****

*Electrical and Electronic Engineering, Khulna University of Engineering and Technology, Khulna-9203, Bangladesh

**Klingler College of Arts and Science, Marquette University, WI 53233, USA

***Department of Electrical Engineering & Renewable Energy, Oregon Tech., Assistant Professor, OR-97601, USA

****Department of Electrical & Electronics Engineering, Gazi University, Faculty of Technology, 06500, Turkey

( jakirhossain471@gmail.com, nazmus.sakib@marquette.edu, eklas.hossain@oit.edu, bayindir@gazi.edu.tr )

‡ Corresponding Author; Third Author, OR-97601, Tel: +1-541-885-1516,

Fax: +1541-885-1689, eklas.hossain@oit.edu

*Received: 19.11.2016 Accepted:17.02.2017*

**Abstract-** To meet the demand of the next generation power system, renewable energy resources can be the fuel of choice because it is easily available, free of cost, environment-friendly, and the renewable energy-based generation is cost effective in all manners. There are several types of renewable energy resources such as solar, wind, geothermal, tides, and biomass. In this paper, the concentration is limited to the solar energy resources, solar plants, and storage system to provide required power support. In particular, this letter is associated with the mathematical modeling of the solar plants and simulation for the different aspects and cases of the system. Besides that, the Zinc Bromide Battery and Li-ion Battery are delineated with the explanations on their performance and related simulations. After that, both for the cases of islanded mode and grid-tied mode operation, the performance of the microgrid systems along with the storage unit are analyzed for different parameters. All the results are verified by Matlab simulations meticulously.

**Keywords** Renewable Energy, Microgrid Systems, Solar Energy, Solar Plant, Storage System, Zinc Bromide Battery, Li-ion Battery.

**Nomenclature and Abbreviation:**

| Abbreviation | Elaboration | Nomenclature | Elaboration | Unit |
|---|---|---|---|---|
| PV | Photovoltaic | OCV | Open Circuit Voltage | Volt |
| CERTS | Consortium for Electricity Reliability Technology Solution | VT | Thermal Voltage | Volt |
| EV | Electric Vehicle | ISC | Short Circuit Current | Ampere |
| OCV | Open Circuit Voltage | Iself discharge | Self discharge Current | Ampere |
| SOC | State of Charging | Rinternal | Internal Resistance | Ohm |
| MPPT | Maximum Power Point Tracking | Vbatt | Terminal Voltage | Volt |
| PI | Proportional Integral | Vo | Output Voltage | Volt |

## 1. Introduction

There are four certain challenges to meet the next generation power demad. First, though the demand is continually incresing, the combustible fossil fuel has almost been depleted because it has been contributing as the primary fuel source since the begining of electrification. Second, the more the combustion, the more the carbon emission, hence the combustible fuel based-power generation causes serious environmental problem. Apart form that, the depletion of the fosil fuel will lead to geological imbalance. Third, the continually increasing cost of the fossil fuel thwarts the industrial and economical progress of the twenty first century. And last but not the least, the power system-in order to meet the higher demand- is now at the stage to shift the choice of fuel. Though the combustible has almost been depleted, the renewable energy-based power generation is the blessings that can meet the chaallenges mentioned above [5]. Renewable energy resources are environmental friendly, free of cost, easily available in the environment, and nondepletable. Almost 17-20% energy demand all over the globe is currently meeting by using renewable energy resources. The figure 1 depicts the renewable energy production all over the world.

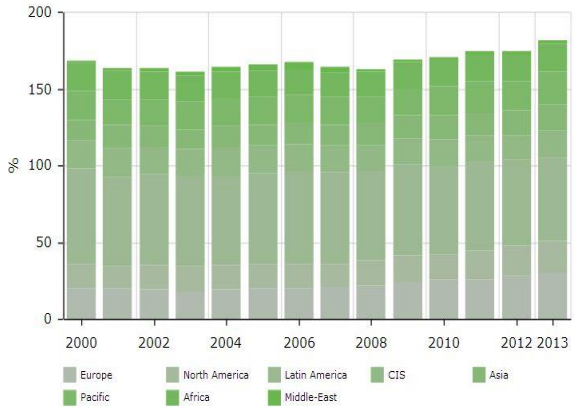


**Fig. 1.** Renewable energy production all over the world.

To implement the renewable energy based-electricity generation, microgrid system has been adopted around the world. Microgrid system integrates several types of renewable energy sources, such as solar system (PV), wind turbine, fuel cell, to the household and industrial load [6, 7]. It is a locally arranged distributed generation-based system and it requires secure communication for safe and uninterrupted generation. To enhance the efficiency of the renewable energy-based generation and eventually the net power generagion by using renewable energy sources, a number of researches have been carried out all over the world [15-17, 20]. In particualr, Some of the renowned microgid testbed are the Consortium for Electricity Reliability Technology Solution (CERTS), Georgia Tech microgrid, University of Texas Arlington microgrid, Microgrid testbed at Albuquerque New Mexico, British Columbia Institute of Technology Microgrid, Kyoto eco-energy microgrid etc and they are conducting top-notch research to enhance the system efficiency of the renewable energy-based microgrid systems. In this occasion, University of Wisconsin-Milwaukee has also endeavoured to find some new approaches to develop a microgrid system [13-14]. In this study, several types of renewable sources have been used to design a microgrid. These are PV system, wind turbine, fuel cell etc. The powers (rated) of the plants are 100 kW, 12 kW, and 50 kW in sequence. The wind turbine consists of 12 kW PMSG. The solar plant is modeled with a number of series and parallel connections [8, 19]. Here, 20 PV arrays are connected in parallel of series arrays containing 10 panels in each of the groups. According to the parameters of 50 kW rated power, the fuel cell stack is also modeled. The wind turbine is operated according to the various wind. To validate the MPPT algorithm, the irradiation of the solar plant are planned to oscillate between the values of 600 W/m2 and 1400 W/m2 [4].

In this paper, the concentration will be limited to the solar energy resources, PV systems, Solar plants, and storage systems. The contribution of this paper is as follows. In section two, the microgrid model is presented. Later, in section three, the solar plant modeling is presented including the charcteristics of solar cell, I-V characteristics of the PV module, PV array with MPPT function, Solar irradiation profile and output power (For perfect day), Implementation of MPPT (For perfect day), Implementation of MPPT (For cloudy day). In section four and five, the Zinc Bromide Battery and Li-ion Battery are delineated considering several aspects and conditions. Finally, in section six, the simulation and analysis are delineated for certain parameters in the case of islanded mode of microgrid operation and grid-tied mode operation where soalr plants are used as one of the sources of renewabe energy-based power generation.

## 2. Microgrid Model

Microgrid system, in a locally adopted setup, incorporates several distributed generation units including the renewable resources and more importantly it is possible to operate the microgrid system autonomously [18].

The sources of microgrid generation are wind energy, solar energy, fuel cells and other energy sources. To run it autonomously and as per the requirements of any circumstances of demand, the multiple and isolated sources of microgrid makes it feasible. In figure 2, the microgrid system is modelled with the renewable energy sources and some storage system. In this figure, a 12 kW wind turbine, 100 kW solar panel, two 45 kW natural gas generator, and 50 kW fuel cell are connected to a bus-bar in left side, which is known as source side. And on the right side of the bus-bar, several loads are connected such as the electric vehicle charging station, 200 kW passive load etc.

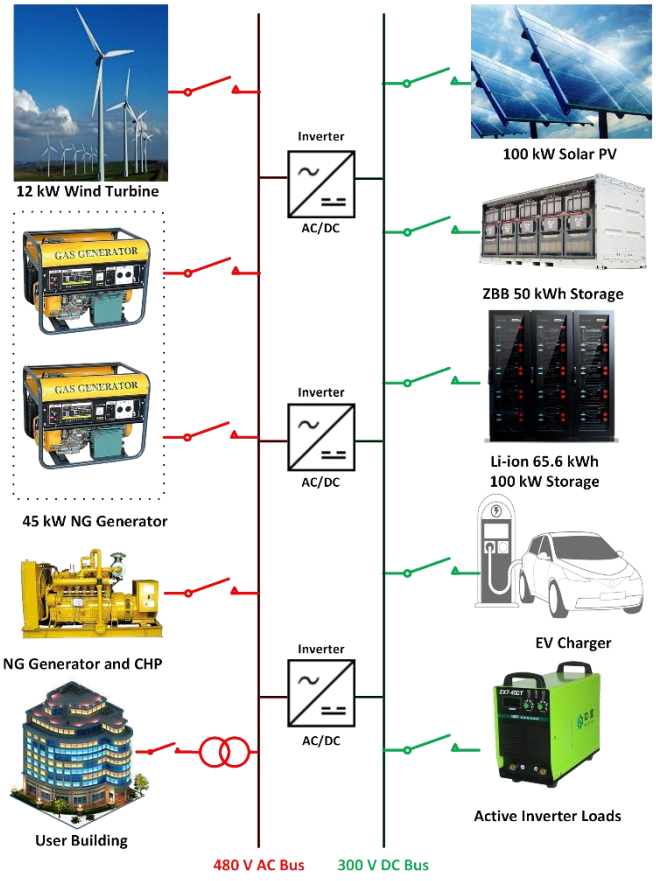


**Fig. 2.** University of Wisconsin Milwaukee Microgrid Testbed.

## 3. Solar Plant Modeling

PV cell can be modeled by considering that a diode in which light in the form of photons with appropriate energy levels falls on the cell and creates electron-hole pairs. Electric field is mainly responsible to separate the electrons and holes in junction diode and drive around the external circuit by this potential. A commonly used equivalent circuit of solar cell with a schematic diagram of a solar cell is shown in figure 3.

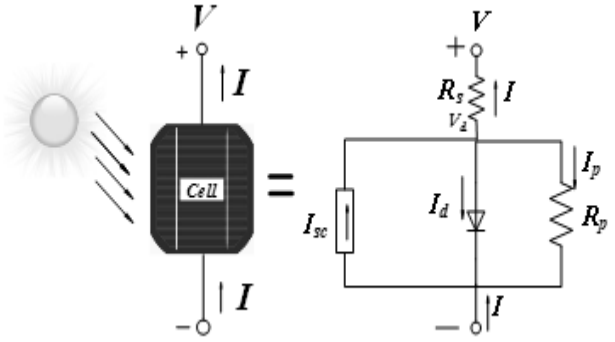


**Fig. 3.** Equivalent circuit of solar cell [11].

The output current and output voltage relation of a solar cell may be derived from the equivalent circuit of figure 3 and can be represented as equation (1).

$$I_o = I_L - I_{Rs}\left(\left[\exp\left(\frac{V_O + I_o R_s}{\eta_I V_T}\right) - 1\right] - \frac{V_O + I_O R_S}{R_{sh}}\right) \quad (1)$$

A solar panel model is built in Simulink by using the analytical equation of a photovoltaic (PV) cell shown in figure 3. In the case of solar cell, the maximum power Pmax, maximum power current Ipmax, and maximum power voltage Vpmax are specified by the manufacturers [3,11]. Table 2 illustrate the standard test condition 1000 w/m2 Irradiance, 25 0C Cell Temperature, which is used for the simulation study.

**Table 1.** Parameter for 100 kW SANYO HIT Power 210N Photovoltaic Module.

| Photovoltaic Module SANYO Electric Co., Ltd | |
|---|---|
| 1000 w/m² Irradiance, 25 °C Cell Temperature | |
| Parameter | Nominal Values |
| Maximum Power $P_{max}$ | 210 W |
| Short Circuit Current $I_{SC}$ | 5.57 A |
| Open Circuit Voltage $V_{OC}$ | 50.9 V |
| Maximum Power Current $I_{pmax}$ | 5.09 A |
| Maximum Power Voltage $V_{pmax}$ | 41.3 V |
| Maximum System Voltage | 600 V |
| Temperature Coefficient (Pmax) | 0.336%/ °C |
| Temperature Coefficient (Voc) | 0.142 V/ °C |
| Temperature Coefficient (Isc) | 1.95 mA/ °C |
| Cell Efficiency | 18.9% |
| Module Efficiency | 16.7% |

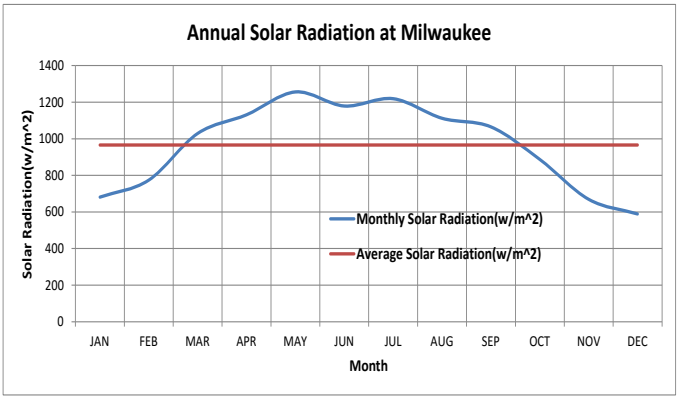


**Fig. 4.** Annual solar radiation curve for Milwaukee.

To implement the solar cell power generation in proposed microgrid model, the annual variation of solar irradiation profile over the Milwaukee area is studied and represented in

figure 4. The yearly average solar irradiation is almost 990 w/m2 and the maximum energy density occurs from the May to July session of the year. The maximum insolation is 1230 w/m2.

### *3.1. Characteristics of solar cell*

Some specific parameters determine the electrical power output of a PV cell. Required number of PV cells are connected in series and parallel configuration to make the solar panel module. A solar panel model is verified by observing the power and the current-voltage (I-V) curves for certain irradiation values. Solar panel models are subjected to irradiations from 200 W/m2 to 1000 W/m2 to obtain the curves shown in figure 5 to figure 9. PI control is added to standard perturbation for the Maximum Power Point Tracking (MPPT) and the algorithm is observed at the region where the response time decreases [3].

#### *3.1.1. Effect of temperature:*

Output characteristics of a solar PV in the case of temperature variation is shown in Figure 5. From this depiction, it is evident that the output current of a solar PV is almost independent of the temperature variation and there is a slightest change in output voltage introduced [10] as shown in figure 5 for the increase in temperature 25oC to 60oC, output voltage increases gradually.

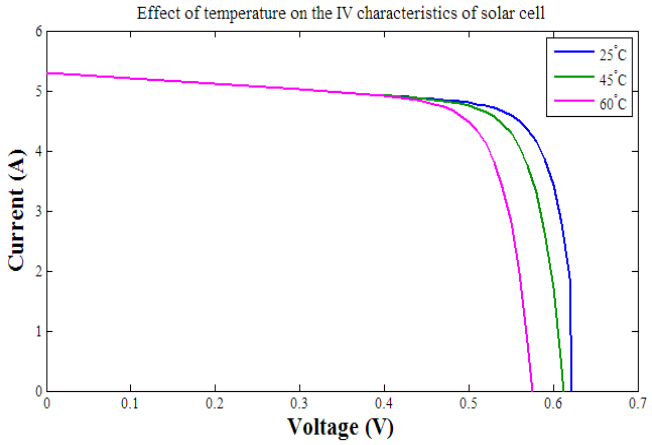


**Fig. 5.** Temperature effect curve.

#### *3.1.2. Effect of Series Resistance:*

The output current of solar PV is limited by the equivalent series resistance of the cell. The dependence of series resistance on output characteristics of a solar PV is tested for various values of series resistance, it is found that the output current gradually decreases with the increase of series resistance [11] as presented in figure 6.

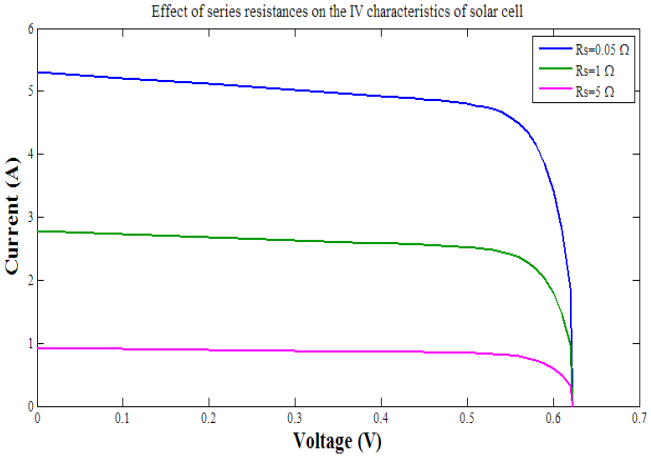


**Fig. 6.** Effect of series resistance.

#### *3.1.3. Effect of Series and Parallel resistances:*

For the better performance of a solar PV cell, the lower the value of series resistance and the higher the value of parallel resistance is desirable. Figure 7 shows the combined effect of the series and parallel resistance on solar PV cell. For the infinite parallel resistance and the zero series resistance, the appreciable output characteristics may be obtained.

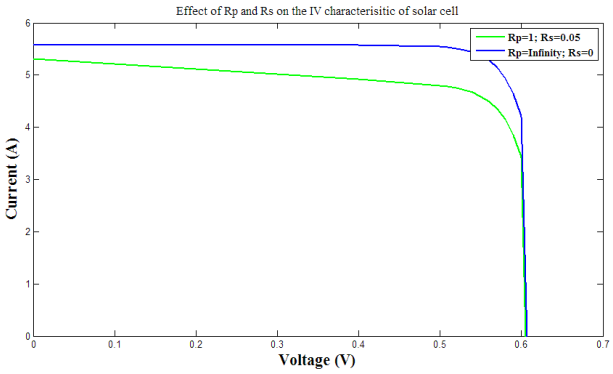


**Fig. 7.** Effect of series and parallel resistance.

#### *3.1.4. Effect of reverse saturation current:*

Reverse saturation current of a diode is the deviating flow of minority carrier from the p-side to the n-side and vice versa. It depends on the diffusion coefficients of the carriers which means it is highly sensitive to the temperature changes and independent of the reverse biasing. The effect of the reverse saturation current on output characteristics of a solar PV is presented in figure 8.

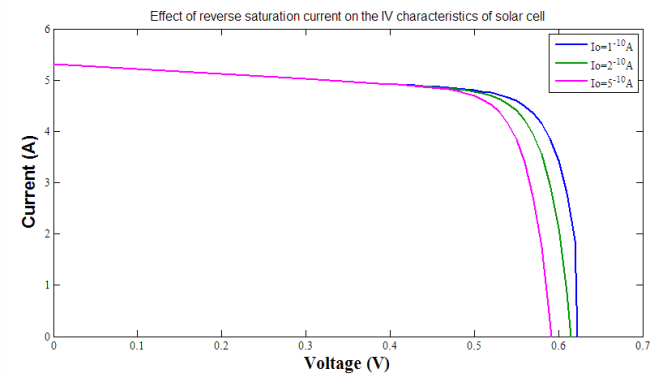


**Fig. 8.** Effect of reverse saturation current.

### 3.1.5. *Effect of ideality factor:*

The ideality factor of a solar PV is the degree of closeness of its output characteristics to its ideal characteristics [10]. A solar PV have been tested for various ideality factors and the summarized result is represented in figure 9. The output voltage of the solar PV linearly increases with its ideality factor while the current variation remains independent.

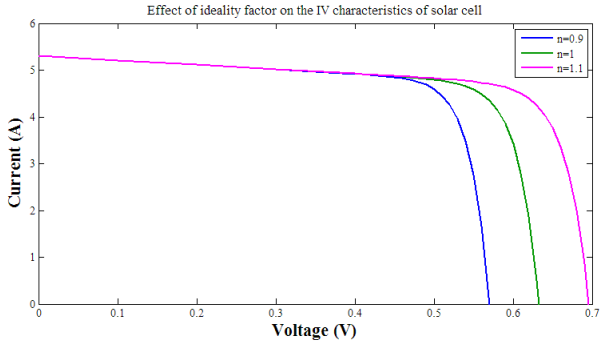


**Fig. 9.** Effect of ideality factor.

### 3.2. *I-V characteristics of PV module*

The I-V characteristics (Blue) and the power output (Pink) for a single solar PV cell is presented in figure 10. Here, the output power is scaled down to 1/15th times of its original value. The I-V characteristics (Blue) and the power output (Green) for the entire solar PV array are illustrated in figure 11. Here, the output power is scaled down to 1/200th times of its original value. The I-V characteristics of 100kW solar PV array for our microgrid model is estimated and represented in Figure 12. Here, the output voltage is almost 560 volt and output current is 250 ampere.

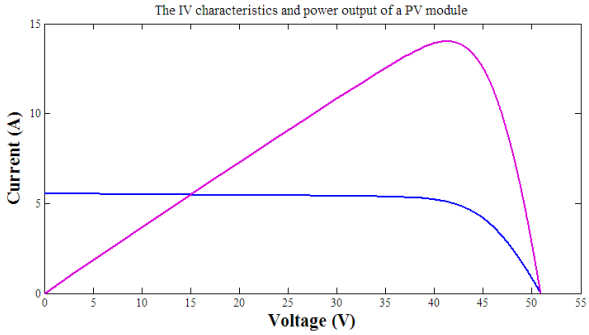


**Fig. 10.** The I-V characteristics of PV module.

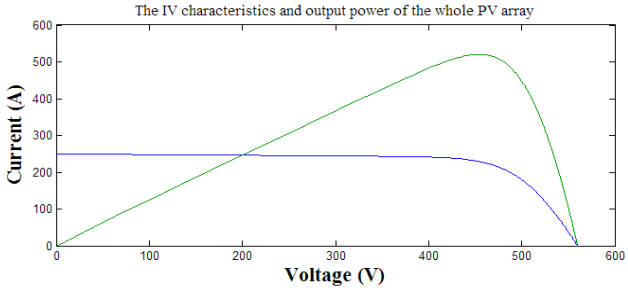


**Fig. 11.** The I-V characteristics of the entire PV module.

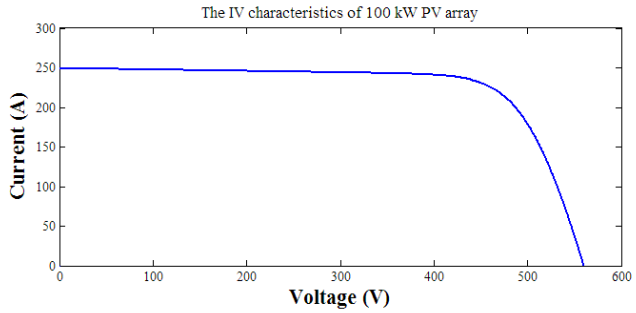


**Fig. 12.** The IV characteristics of 100 kW PV array.

### 3.3. *PV array with MPPT function*

A solar PV array model with the implementation of Maximum Power Point Tracking function is presented in Figure 13.

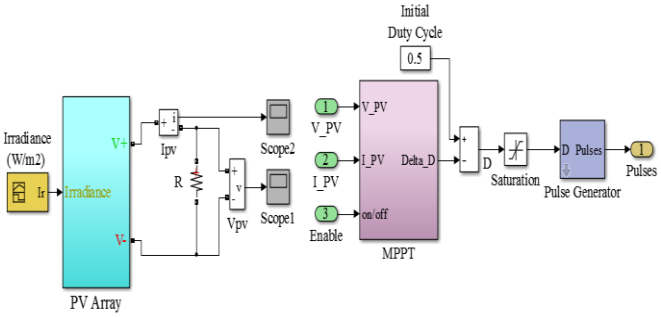


**Fig. 13.** The PV array and MPPT function.

### *3.4. Solar irradiation profile and output power (For perfect day)*

The solar irradiation profile for a perfect day and the corresponding output power of the solar PV array along with the output voltage and the output current are depicted in figure 14 and figure 15. Here, the required time is scaled down to 1/8th times of its original value.

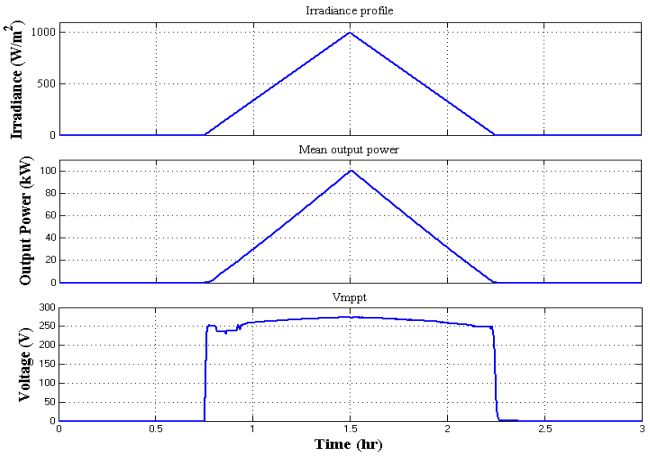


**Fig. 14.** The solar irradiation profile and the output power of the PV array.

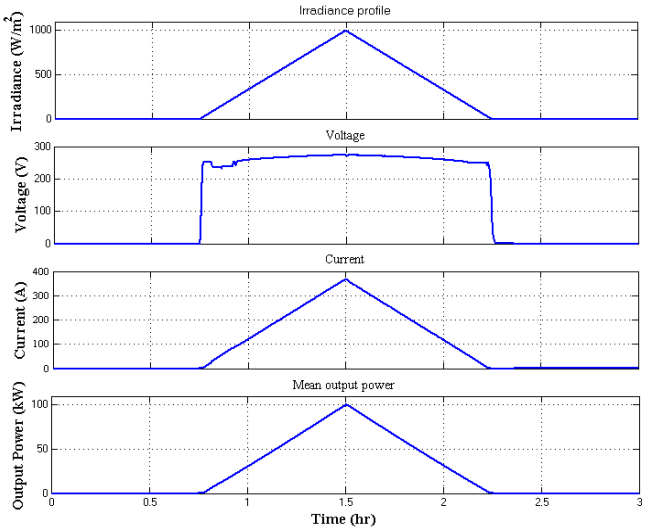


**Fig. 15.** Voltage, current and output power variation with irradiation.

### *3.5. Implementation of MPPT (For perfect day)*

From the irradiation and the output characteristics, it is seen that the solar PV generates power for a specific period of the day. By implementing the MPPT function, a duty cycle may be defined for the solar PV operation. Figure 16 shows the duty cycle generation for a solar PV array (for a perfect day). Figure 17 illustrates the implementation of the MPPT function using incremental conductance and integral regulator. Here, the time is scaled down to 1/8th times of its original value.

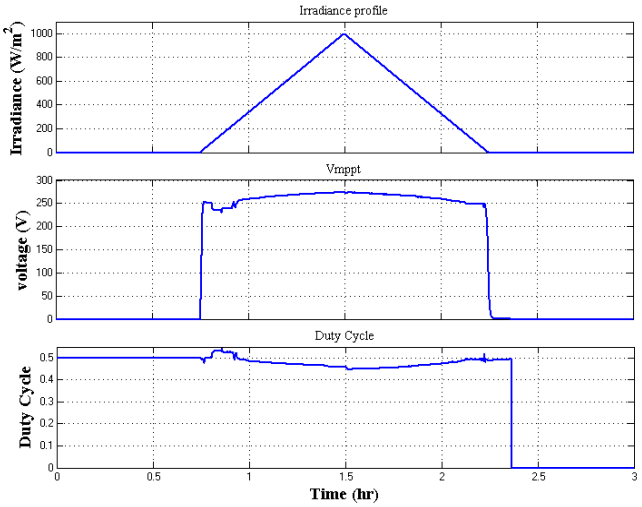


**Fig. 16.** Duty cycle generation using MPPT.

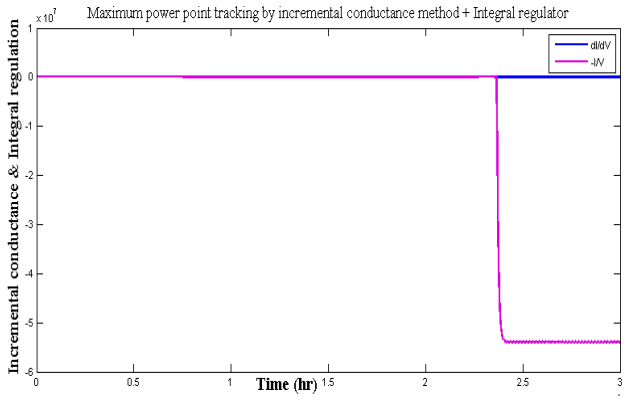


**Fig. 17.** Incremental conductance & Integral regulator.

### *3.6. Solar irradiation profile and output power (For cloudy day)*

The solar irradiation profile for a cloudy day when irradiation varies unpredictably is shown in figure 18, and with the variation of the output power, output voltage, and the output current in figure 19.

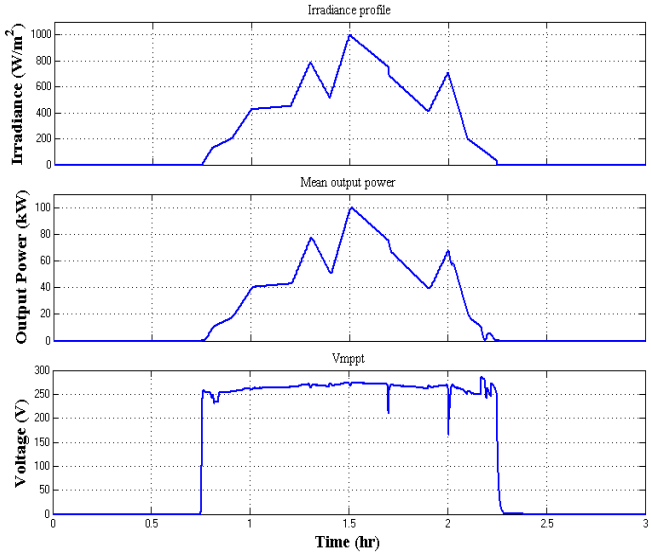


**Fig. 18.** The solar irradiation profile and output power of the PV array.

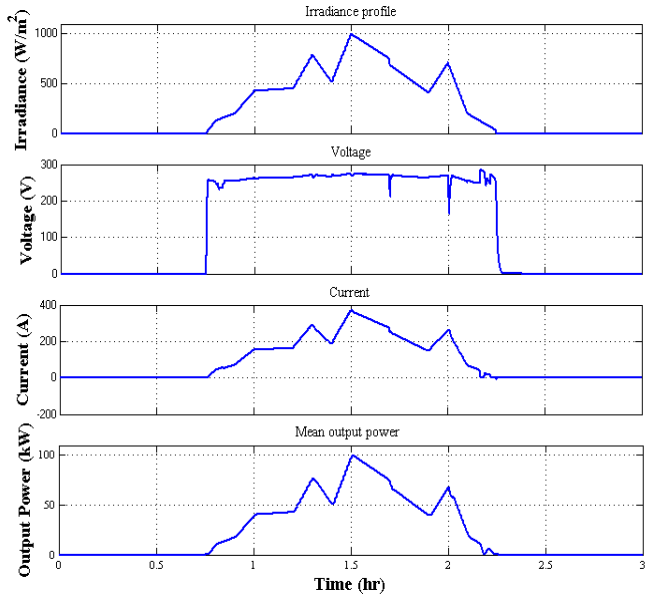


**Fig. 19.** Voltage, current, and output power variation with irradiation.

### 3.7. *Implementation of MPPT (For cloudy day)*

Duty cycle generation for cloudy day using MPPT function is shown in figure 20 and the implementation of MPPT function using incremental conductance and integral regulator are in figure 21.

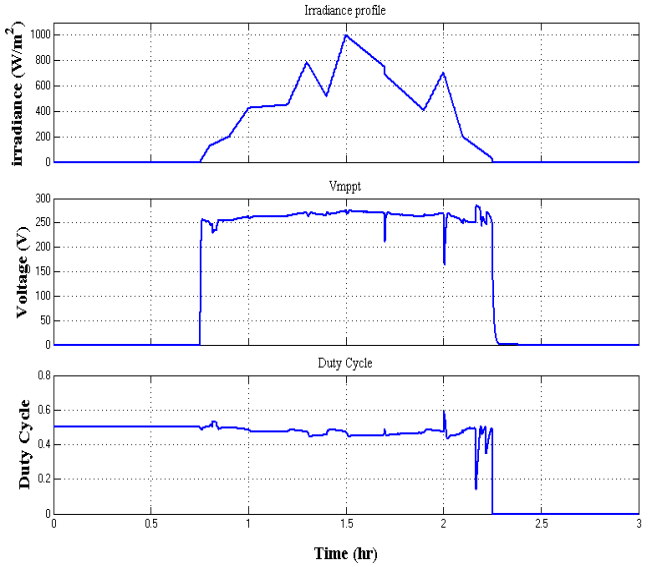


**Fig. 20.** Duty cycle generation using MPPT.

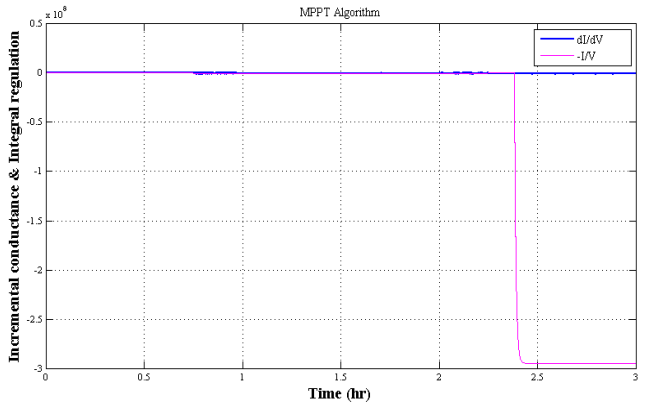


**Fig. 21.** Incremental conductance & Integral regulator.

## 4. Zinc Bromide 50 KWH Storage

Compared to the 750 cycles of the conventional lead acid batteries, the zinc bromide battery can practically surpass the 2000 full charge and discharge cycles in its operating lifespan. In particular, it is able to have full discharge without any kind of damage to the battery (100% of stored energy). Besides that, its energy density lies inbetween 65–84W h/kg, and it can operate at a wide operating temperature range without any significant deterioration. While manufacturing, the costs can be scaled down by making the components using plastic materials entirely, it also provides the ability of quick disposal or recycling. and provide readily for recycling or disposal. Furthermore, it uses not only a electrolyte with low toxicity, but also a battery stack made with plastic that makes it recyclable, hence much environmental friendly compared to the conventional one made with more noxious sulfuric acid and lead [1]. Here, the electrolyte is a zinc bromide water solution (ZnBr2 + H2O), quaternary ammonium salts, and supporting salts to decrease the reistivity. Figure 22 depicts the electrolyte flow diagram.

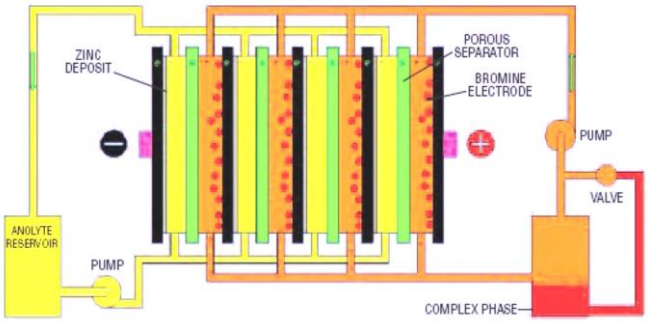


**Fig. 22.** Flow of electrolyte in a Zinc-Bromide energy storage system [1].

As has been seen form this figure, two reservoirs are used to store the electrolyte. Between these two, one is used as anolyte and the other one makes the catholyte. Here, a lot of cells is used to make a battery, with 1.83 V being the nominal voltage of a cell. İn the case of charging and discharging, the underlying electrochemical reactions are:

$$Zn^2 + 2e^- \rightarrow 2Zn$$
$$2Br^- \rightarrow Br_2 + 2e^-$$

As seen in figure 22, zinc is electrochemically plated on the electrode's smooth side through the given reaction process. Then, Bromine is synthesized at the cathode, accompanied by the free electrons. In the time discharge, a secondary pump is used to return the polybromide liquid to the cell stacks by pulling the dense liquid from the bottom of the reservoir. In case of complete discharge, the polybromide complex is converted to a solution (ZnBr2 + H2O) and quaternary ammonium salts; zinc ions are produced by oxidizing zinc, and bromide ions being made from bromine [1]. In table 2, conventional batteries and the Zinc Bromide energy storage are compared on several parameters.

**Table No. 2: Comparison of properties of Zinc Bromide energy storage with other batteries.**

| Battery | Energy Density (Wh/kg) | Power Density (W/kg) | Cycle Life |
|---|---|---|---|
| **Lead-Acid** | 30-50 | 100-200 | 200-300 |
| **Lithium-Ion** | 150-190 | 300-1500 | 300-500 |
| **Nickel Metal Hydrate** | 60-120 | 250-1000 | 300-500 |
| **Zinc-Bromide** | 85-90 | 300-600 | 2000 |

A Zinc Bromide bettary unit having specification mentioned above is modeled using MATLAB/Simulink as showen in figure 23.

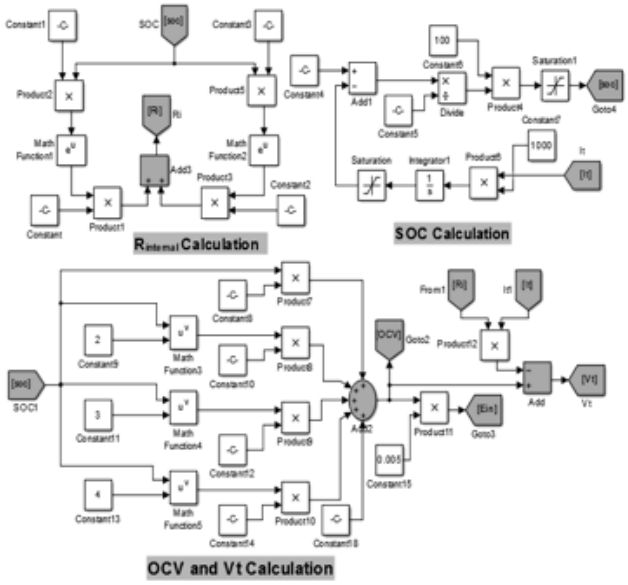


**Fig. 23.** The Zinc Bromide Battery design in Simulink.

Here, the block wise representation is presented seperately for the SOC, Rinternal , and OCV calculation. Results from the simulation, Discharge current and % state of charge (SOC) are represented in figure 24. In which, the battery is completely discharged within 25 min where discharge current fall from 80 A to -20 A, after 4 mins of constantly discharging and in the mean time SOC fall from 100% to 25% than again start rising upto 100% within the next 16 min and remains constant the rest of the time.

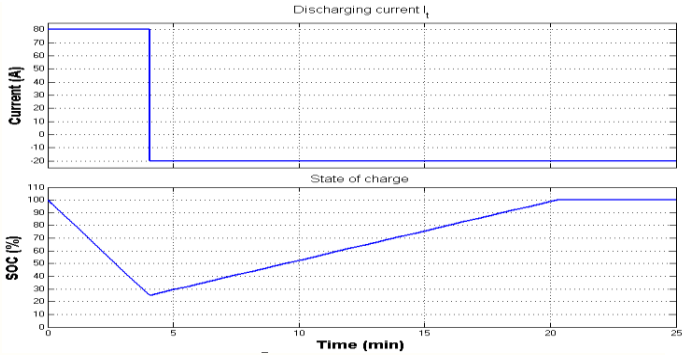


**Fig. 24:** The waveform of charging current and SOC in percentage.

In this simulation, the nominal capacity of the ZBB used is (72*1.67*3600=102 Amp-hr=) 432000 Amp-sec. The SOC is determined from the following equation:

$$SOC = 1 - \int_0^t i_t * dt \quad (2)$$

In this simulation, the constant current charging and discharging technique is used. While the discharging current is constant, the SOC decreases and starts to increase while the charging current is kept constant. The Open Circuit Voltage (OCV) and the terminal voltage of the battery unit from the Simulink model is presented in the figure 25 for 25 mins of the constant rate discharging situation.

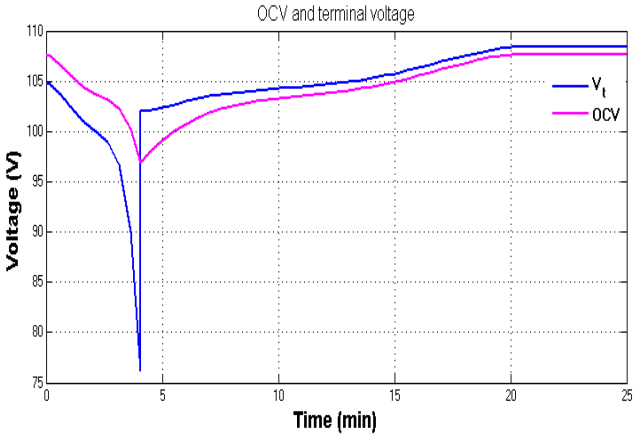


**Fig. 25.** The waveforms of OCV and terminal voltage.

The electrical equivalent circuit of ZBB cell is presented in the figure 26 where OCV, Iself discharge and Rinternal are the function of SOC.

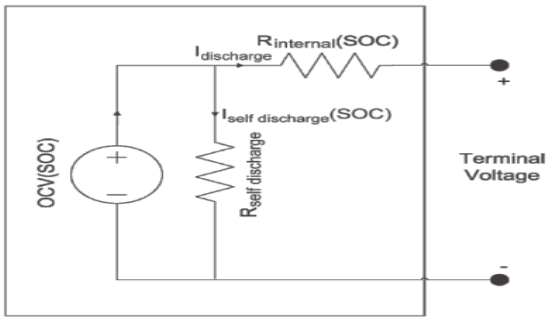


**Fig. 26.** The electrical model of the ZBB.

The terminal voltage from the equivalent circuit can be determined by the following equation.

$$V_t\,(SOC) = OCV\,(SOC) - R_{internal}\,(SOC) * i_t \qquad (3)$$

Terminal voltage is dependent upon the SOC. It reduces while the SOC decreases and starts to increase again if the charging current is applied. Figure 27 represents the dependence of OCV with SOC.

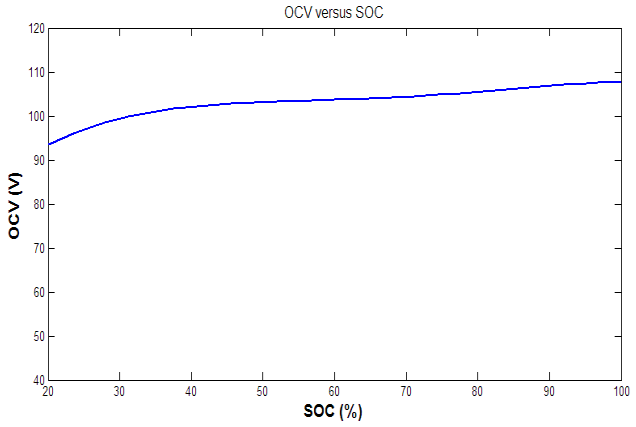


**Fig. 27.** The curve of OCV versus SOC.

The OCV may be determined by the 4th order polynomial function of SOC given as equation (4).

$$OCV(SOC) = 1.8781 * 10^{-6}.SOC^4 + 5.2857 * 10^{-4}.SOC^3 - 0.0535.SOC^2 + 2.3386.SOC + 63.0936 \qquad (4)$$

The open circuit voltage (OCV) increases with the increase in SOC as the 4th order polynomial function of SOC. The internal resistance is a function of many variables, but it mainly depends on the cell and the ambient temperatures as well as the SOC [1]. Figure 28 represents the dependence of Rinternal with SOC. According to the test data, an exponential function representing Rinternal is obtained from equation (5).

$$R_{internal}(SOC) = 5.9415e^{-0.13493.SOC} + 0.0254e^{-5.7711*10^{-3}.SOC} \qquad (5)$$

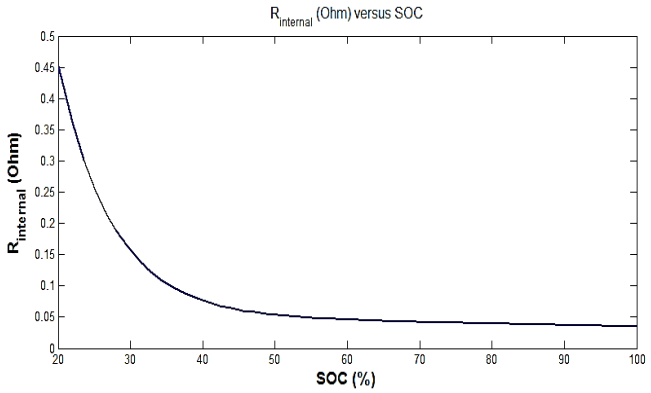


**Fig. 28.** The curve of $R_{internal}$ versus SOC.

A parallel resistance with the OCV source can model the self-discharging. The self-discharging resistance can be calculated [1] by equation (6).

$$R_{self-discharging} = \frac{OCV(SOC)}{I_{discharging}} = \frac{OCV(SOC)}{\Delta q_{lost}/\Delta t} \qquad (6)$$

The self-discharging resistance is supposed to be constant, independent of SOC. To overcome this glitch, an average value for the self-discharging resistance was found by

averaging the resistance curve. This method provides a self-discharging resistance of 5.1 Ω [8]. The dependence of self-resistance with SOC is shown in figure 29.

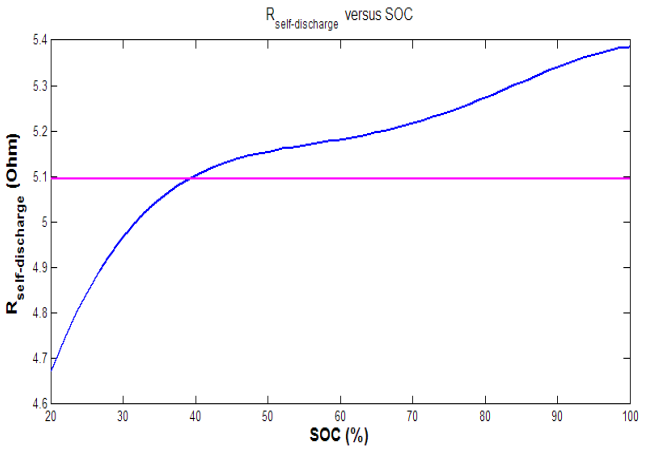


**Fig. 29.** The curve of $R_{self\text{-}discharging}$ vs. SOC.

## 5. LI-ion Battery

A lithium-ion battery system is reliable and has high power performance, symmetrical charge and discharge capability, wider operational temperature capabilities, longer cycle life, and higher safety aspects along with compact size. To comprehend the nature of the EV's batteries, Electric Circuit (EC)-based battery models are used. This section illustrates the equivalent circuit-based battery model of the f Lithium-ion (Li-ion) battery, and its mathematical delineation [2].

### *5.1. Battery Equivalent Circuit*

The electrical equivalent circuit of a Li-ion battery unit is depicted in the figure 30 which presents the EC-based battery model. Here, R1 and R2 of the circuit are the internal resistance, C the internal capacitance, Vbatt and Vo the terminal and open circuit voltages of the battery respectively [2].

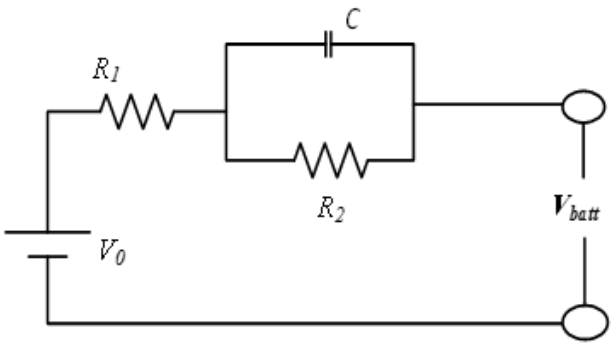


**Fig. 30.** Equivalent circuit for Li-ion battery [2].

The parameters R1 , R2 , C and Vo can be expressed by the polynomial equations to delineate the nonlinear phenomenon of the battery.

### *5.2. Charge/Discharge Model:*

Figure 31 illstrates the block representation of the battery model in the time of charging and discharging phenomenon. This model is constructed by using the polynomial equations above. The input given to the model are constant current (I ), initial capacity of the battery (Q), nominal voltage (V), time taken (t), charge (Cr ) and discharge (Dr) rate. If the current is positive, charging takes place and when the current is negative, the battery discharges. The output of this model is Vbatt, if the battery is discharging. The output of this model is VO , if the battery is charging [2].

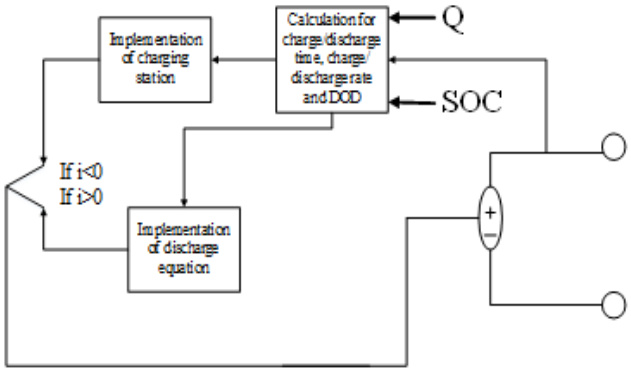


**Fig. 31.** Schematic representation of charging and discharging conditions.

Here, the battery is connected to a constant load of 50 Amps. Besides that, the DC machine is connected with the load in parallel connection and operates at no-load torque. When the SOC of the battery goes below 0.4 (40%), a negative load torque of 200 Nm is applied to the machine. Hence, it bahaves as a generator to recharge the battery. When the state of charge goes over 80%, the load torque is removed. Therefore, only the battery supplies the 50 amps load. When the mechanical torque of -200 Nm is applied to the machine, it provides a current of 100 amps. So, 50 amps goes to the load and 50 amps goes to recharge the battery. A MATLAB/Simulink model is presented in figure 32. The nominal current discharge characteristics at 41.304 A and 0.43478 C of the LI-ion battery unit is presented in figure 33. Discharging characteristic at different rate is also evaluated.

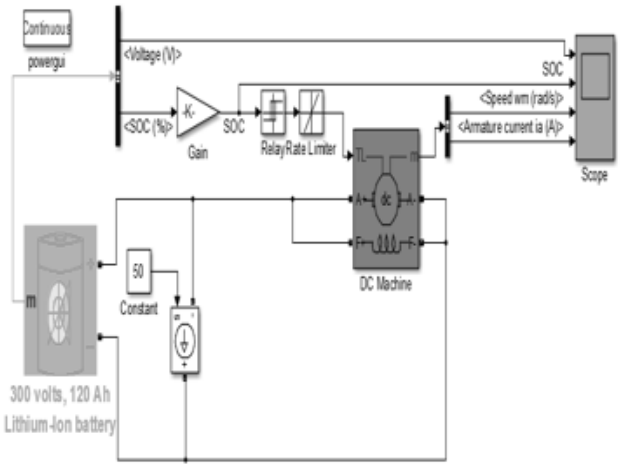


**Fig. 32.** Lithium-Ion battery.

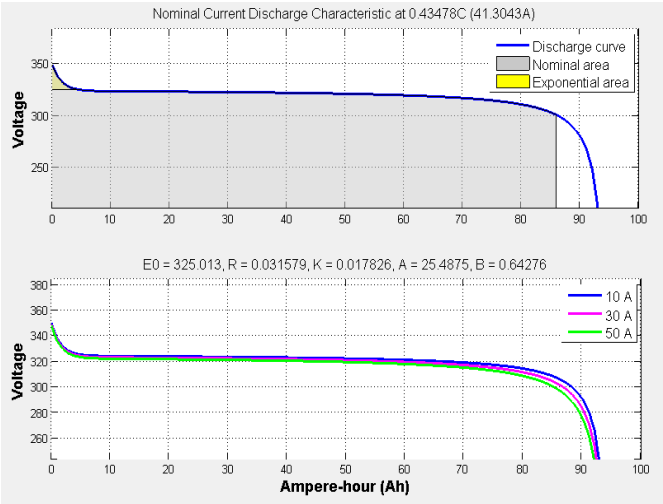


**Fig. 33.** The current discharge characteristics of Lithium-Ion battery.

Percentage SOC variation along with the current and voltage while charging and discharging, the Li-ion battery unit have represented in figure 34. After that, the discharging characteristics for 5000 seconds with the terminal voltage and SOC is shown in figure 35. It is seen from this figure, the terminal voltage remains constant for most of the time.

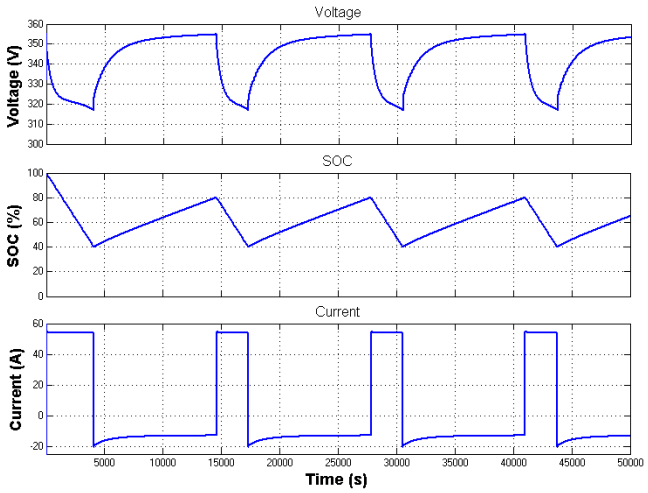


**Fig. 34.** The SOC (%) variation with charging and discharging of Lithium-Ion battery.

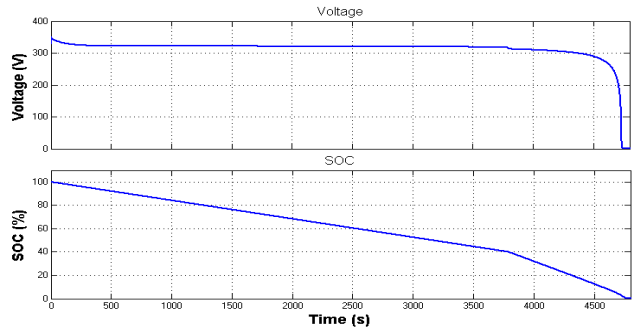


**Fig. 35.** The voltage and SOC variation while discharging of Lithium-Ion battery.

The SOC of the battery ranging between 0 and 100% is shown in the figure 36. The SOC for a fully charged battery is 100% and for an empty battery is 0%. The SOC at any instant of time can be calculated as

$$SOC = 100(1 - \frac{1}{Q}\int_0^t i(t)dt) \quad (7)$$

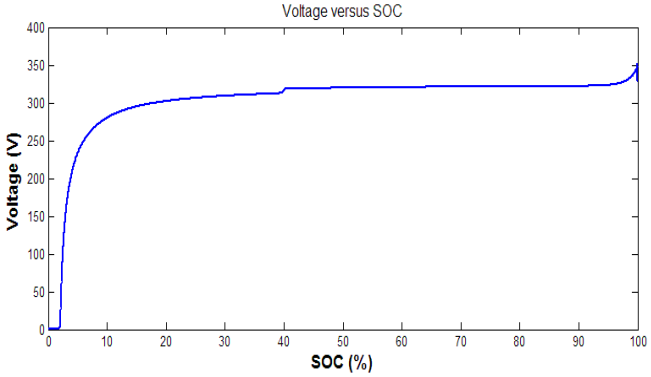


**Fig. 36.** The voltage versus SOC characteristics of the Lithium-Ion battery.

## 6. Simulation and Analysis

A simulation is accomplished for the analysis of 100kW PV array and energy storage units in both Islanded Mode Operation and Grid Tied Mode Operation of designed

microgrid in MATLAB/Simulink Platform. The schematic layout of the simulation model is illustrated in the figure 37 below as block representation.

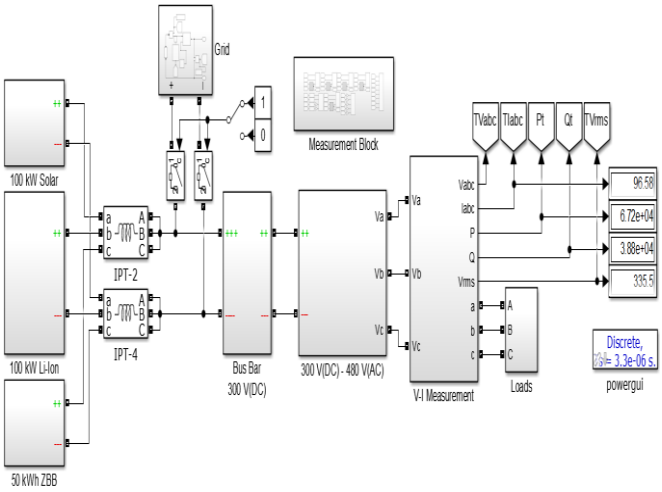


**Fig. 37.** Schematic representation of PV Array and Storage Unit Stand alone/Grid Tied Microgrid Model.

This Photovoltaic model is designed according to the parameters of the Sharp PV panel Ne-170UC1 which supplies 170 W output power. 5 series * 60 parallel Array of 250W, in total 75 kW of maximum output power. The overall simulation is crried out for 1.5 second using solar irrediation profile and IPV Ramp as presented in the figure 38 below.

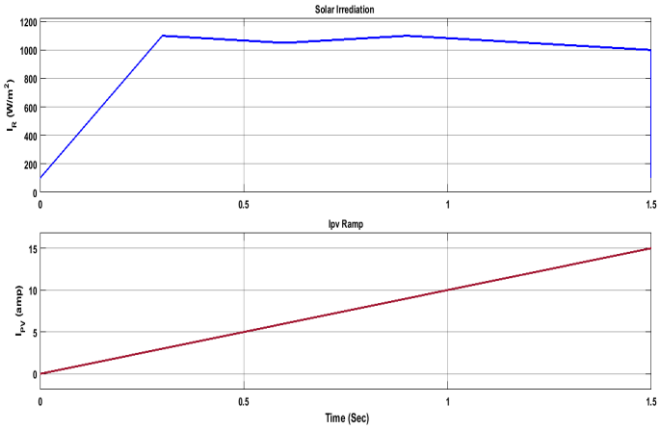


**Fig. 38.** Solar Irrediation profile in w/m2 and IPV Ramp current.

As energy storage unit for backup power in islanded mode operation of microgrid, 100kW Li-ion Battery Storage and 50kW Zinc-Bromide Battery Storage Unit are also modeled as aforementioned avobe and coupled with 100kW PV array using PI controller for energy contribution control. When PV power generation exceedes load deamnd, those battery units are designed to grasp the additional power. The loading profile used for the case study is presented in the figure 39.

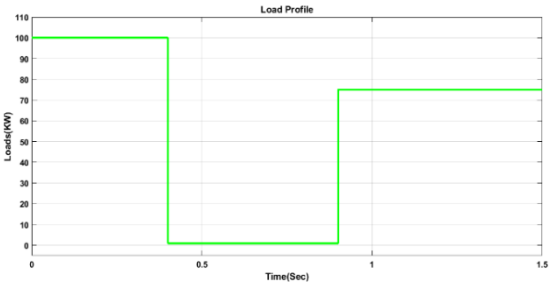


**Fig. 39.** Load Profile.

At first, the simulation environment is set for the islanded mode of operation. After that, the voltage and current characteristics form the various sources is presented in the figure 40. The power contribution from all the sources is showen in the figure 41. As the microgrid is operated in the Islanded mode, the grid coupling breaker is open and the output current from the grid tends to zero as shown in figure 40(f) and the power is also nearly zero as shown in figure 41(b). For the first 0.4 second, the load is set to 100kW which exceeds the PV generation and the storage units provide the additional power for the load demand as shown in the figure 40 and 41. From 0.4 to 0.9, when the loads falls to 1kW, the excess power generated by the PV module is stored by the storage units.

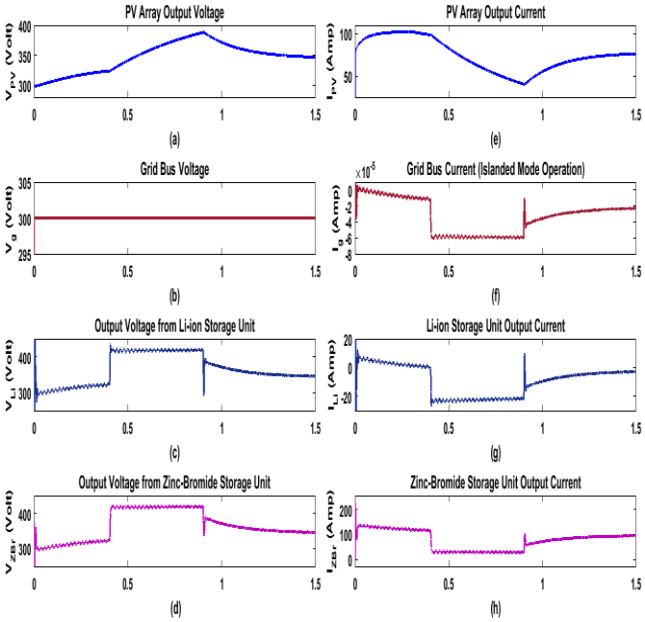


**Fig. 40.** a) PV Array Output Voltage b) Grid Bus Voltage c) Li-ion Storage Unit Output Voltage d) Zinc-Bromide Storage Unit Output Voltage e) PV array Current f) Grid Bus Current g) Li-ion Battery Current h) zinc-Bromide Battery Current for Islanded mode of operation.

To elemenate the harmonics content and avoid the undesirable phenomenon like voltage fluctuations and frequency missmatch, generation from all the different units are coupled with a 300V DC bus bar, then this power is converted to 3phase AC power using 300V DC to 480V AC Inverter unit as shown in the figure 37, before coupling with

the distribution network. The load side characteristics for the standalone microgrid is shown in figure 41. The load side characteristics for the standalone microgrid is shown in the figure 42.

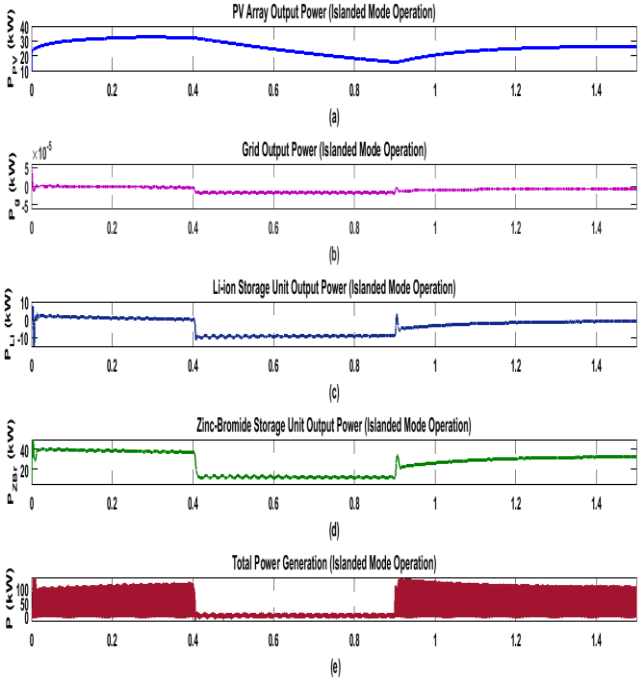


**Fig. 41.** a) PV Array Power b) Grid Power Contribution c) Li-ion Storage Unit Power d) Zinc-Bromide Storage Unit Power e) The overall power generation by the microgrid in Islanded mode of Operation.

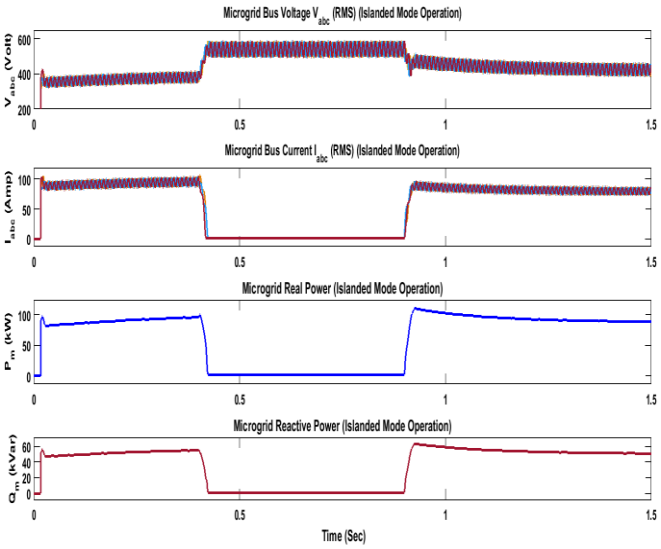


**Fig. 42.** a) Microgrid Bus Voltage (RMS) b) Load Current c) Real Power d) Reactive Power in Islanded mode of operation.

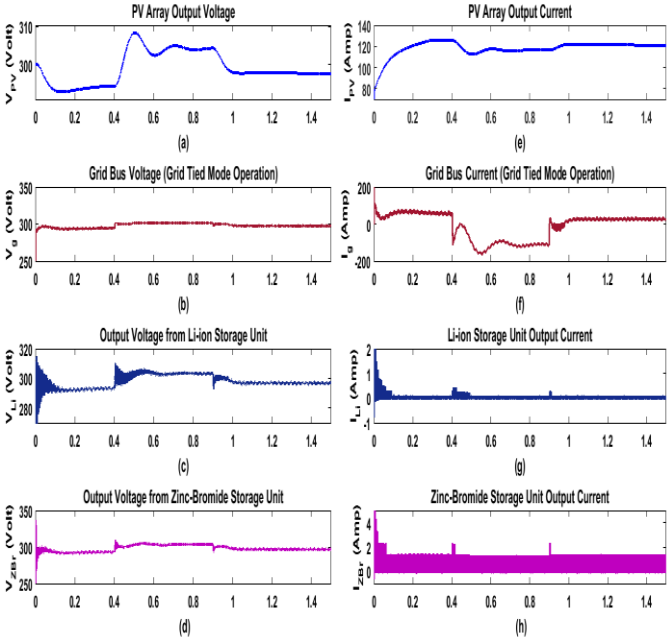


**Fig. 43.** a) PV Array Output Voltage b) Grid Bus Voltage c) Li-ion Storage Unit Output Voltage d) Zinc-Bromide Storage Unit Output Voltage e) PV array Current f) Grid Bus Current g) Li-ion Battery Current h) zinc-Bromide Battery Current for Grid Tied mode of operation.

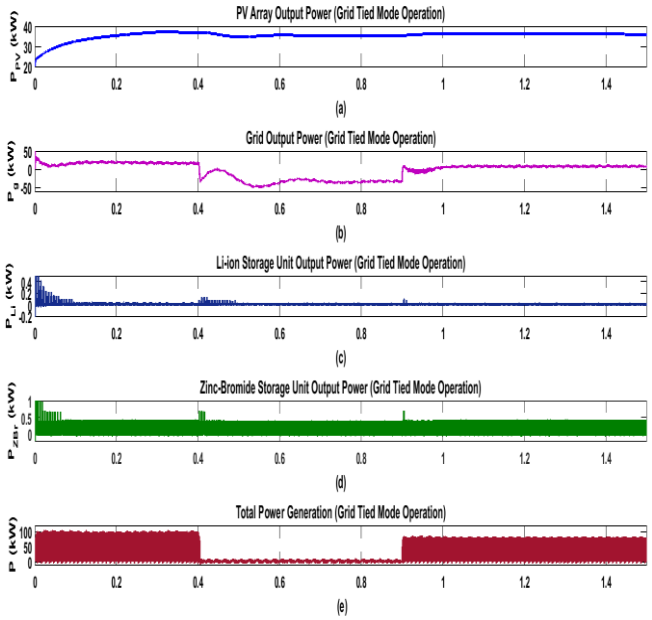


**Fig. 44.** a) PV Array Power b) Grid Power Contribution c) Li-ion Storage Unit Power d) Zinc-Bromide Storage Unit Power e) The overall power generation by the microgrid in Grid Tied mode of Operation.

The simulation is carried out for the Grid Tied Mode of Operation of the designed microgrid in the case of same load profile as mentioned in the figure 39 and of the same simulation time. The voltage and current characteristics for all

available sources in the Grid Tied Mode of operation is presented in the figure 43, and the power output from all the sources is shown in the figure 44. As the microgrid is set to the grid tied mode, the additional power for the load deamnd is supported by the power grid or the utility gid. When the generation exceeds the load demand, the additional power is feed to the utility grid as seen from figure 43 and 44. Contribution from the two storage unit is set to nearly zero as the grid is capable of backing up theoretically infinite amount of power. In particular, at figure 43, a) PV array output voltage, b) Grid bus voltage, c) Li-ion storage unit output voltage, d) Zinc-Bromide storage unit output voltage, e) PV array current, f) grid bus Current, g) Li-ion battery current h) Zinc-Bromide battery current for Grid Tied mode of operation are illustrated. After that, at figure 44, a) PV array power b) Grid power contribution c) Li-ion storage unit power d) Zinc-Bromide storage unit power e) The overall power generation by the microgrid in Grid Tied mode of operation are depicted.

## 7. Conclusion

Besides the negative impact on both the environmental and geological aspect in the case of fossil fuel combustion-based power generation, the fossil fuels have almost been depleted, and hence an alternative fuel source is required. To meet the next generation power demand, renewable energy sources are the most reasonable fuel-shift taken over the naturally limited conventional fuels. Among all the available renewable energy resources, solar energy has been developing as one of the most significant contributors of the power industry. In this paper, the concentration has been limited to the solar energy resources, solar plants, and storage system to provide required power support. In particular, this letter has been associated with the mathematical modeling of the solar plants and simulation for the different aspects and cases of the system. Besides that, the Zinc Bromide Battery and Li-ion Battery have been delineated with the explanations on their performance and related simulations. After that, both for the cases of islanded mode and grid-tied mode operation, the performance of the microgrid systems along with the storage unit have been analyzed for the different parameters. All the simulation results have been demonstrated on the virtual platform such as Matlab/Simulink.

## References

[1] Manla, Emad, Adel Nasiri, Carlos H. Rentel, and Michael Hughes. "Modeling of zinc bromide energy storage for vehicular applications." IEEE Transactions on Industrial Electronics 57, no. 2 (2010): 624-632.

[2] Joy, TP Ezhil Reena, Kannan Thirugnanam, and Praveen Kumar. "Bidirectional contactless charging system using Li-ion battery model." In 2012 IEEE 7th International Conference on Industrial and Information Systems (ICIIS), pp. 1-6. IEEE, 2012.

[3] Kabalci, Ersan, Eklas Hossain, and Ramazan Bayindir. "Microgrid test-bed design with renewable energy sources." In Power Electronics and Motion Control Conference and Exposition (PEMC), 2014 16th International, pp. 907-911. IEEE, 2014.

[4] Kabalci, Ersan, Ramazan Bayindir, and Eklas Hossain. "Hybrid microgrid testbed involving wind/solar/fuel cell plants: A desing and analysis testbed." In Renewable Energy Research and Application (ICRERA), 2014 International Conference on, pp. 880-885. IEEE, 2014.

[5] J. Hossain, S. S. Sikander, E. Hossain, "A wave-to-wire model of ocean wave energy conversion system using MATLAB/Simulink platform," 2016 4th International Conference on the Development in the in Renewable Energy Technology (ICDRET), Dhaka, 2016, pp. 1-6.

[6] Ramazan Bayindir, Eklas Hossain, Ersan Kabalci, and Kazi Md Masum Billah "Investigation on North American Microgrid Facility", International Journal of Renewable Energy Research, Vol.5, No.2, 2015 558-574.

[7] Eklas Hossain, Mashrur Zawad Xahin, Khondokar Rakibul Islam, MD. Qays Akash, "Design a Novel Controller for Stability Analysis of Microgrid by Managing Controllable Load using Load Shaving and Load Shifting Techniques; and Optimizing Cost Analysis for Energy Storage System", International Journal of Renewable Energy Research, Vol 6, No 3 (2016), 772-786.

[8] Manla, Emad, Adel Nasiri, and Michael Hughes. "Modeling of zinc energy storage system for integration with renewable energy." Industrial Electronics, 2009. IECON'09. 35th Annual Conference of IEEE. IEEE, 2009.

[9] Mukhtaruddin, R. N. S. R., H. A. Rahman, M. Y. Hassan, and J. J. Jamian. "Optimal hybrid renewable energy design in autonomous system using Iterative-Pareto-Fuzzy technique. " International Journal of Electrical Power & Energy Systems 64 (2015): 242-249.

[10] Baghzouz, Yahia. "Basic Photovoltaic Theory." Handbook of Clean Energy Systems.

[11] Sayed, Khairy, Mazen Abdel-Salam, Mahmoud Ahmed, and Adel A. Ahmed. "Modeling and simulation of PV arrays." In ASME 2010 International Mechanical Engineering Congress and Exposition, pp. 1113-1120. American Society of Mechanical Engineers, 2010.

[12] Li, Xue, Jiuchun Jiang, Caiping Zhang, Le Yi Wang, and Linfeng Zheng. "Robustness of SOC Estimation Algorithms for EV Lithium-Ion Batteries against Modeling Errors and Measurement Noise." Mathematical Problems in Engineering 2015 (2015).

[13] Eklas Hossain, Ersan Kabalci, Ramazan Bayindir and Ronald Perez "A Comprehensive Study on Microgrid Technology", International Journal of Renewable Energy Research, Vol.4, No.4, 2014 1094–1107.

[14] Eklas Hossain, Ersan Kabalci, Ramazan Bayindir and Ronald Perez “Microgrid testbeds around the world: State of art”, Energy Conversion and Management 86 (2014) 132–153.

[15] Nazmus Sakib, Jakir Hossain, Eklas Hossain, Ramazan Bayindir “Modelling and Simulation of Natural Gas Generator and EV Charging Station: A Step to Microgrid Technology”, International Journal of Renewable Energy Research, Vol. No. 7, Issue No. 1, Pages 399-410, 2017.

[16] Longo M., Roscia, M., Lazaroiu, G.C., Pagano, M., Analysis of sustainable and competitive energy system, 3rd International Conference on Renewable Energy Research and Applications, ICRERA 2014, Pages 80-86.

[17] Longo M., Zaninelli D., Viola F., Romano P., Miceli R., Eletric vehicles impact using renewable energy, 10th International Conference on Ecological Vehicles and Renewable Energies, EVER 2015.

[18] N. Sakib, J. Hossain, H. I. Bulbul, E. Hossain and R. Bayindir, "Implementation of unit commitment algorithm: A comprehensive droop control technique to retain microgrid stability," *2016 IEEE International Conference on Renewable Energy Research and Applications (ICRERA)*, Birmingham, 2016, pp. 1074-1079.
doi: 10.1109/ICRERA.2016.7884499

[19] I. Colak, E. Hossain, R. Bayindir and J. Hossain, "Design a grid tie inverter for PMSG wind turbine using FPGA & DSP builder," 2016 IEEE International Power Electronics and Motion Control Conference (PEMC), Varna, 2016, pp. 372-377.
doi: 10.1109/EPEPEMC.2016.7752026

[20] Eklas Hossain, Jakir Hossain, Nazmus Sakib, Ramazan Bayindir “Modelling and Simulation of Permanent Magnet Synchronous Generator: A Step to Microgrid Technology”, International Journal of Renewable Energy Research, Vol. No. 7, Issue No. 1, Pages 443-450, 2017.